Journal of Materials Chemistry A

Accepted Manuscript

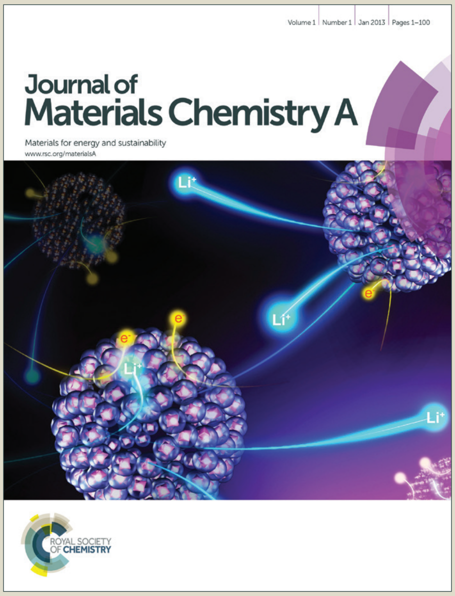

Volume 1 | Number 1 | Jan 2013 | Pages 1–100

Journal of Materials Chemistry A

Materials for energy and sustainability

www.rsc.org/materialsA

ROYAL SOCIETY OF CHEMISTRY

ROYAL SOCIETY OF CHEMISTRY

www.rsc.org/materialsA

Journal of
Materials Chemistry A

RSCPublishing

ARTICLE

High Performance and Negative Temperature Coefficient of Low Temperatures Hydrogen Gas Sensors using Palladium decorated Tungsten Oxide

Cite this: DOI: 10.1039/x0xx00000x

Yanrong Wang,[a] Bin Liu,[a] Songhua Xiao,[a] Han Li,[a] Lingling Wang,[a] Daoping Cai,[a] Dandan Wang,[a] Yuan Liu,[a] Qiuhong Li*[a], Taihong Wang*[a]

Received 00th January 2012,
Accepted 00th January 2012

DOI: 10.1039/x0xx00000x

www.rsc.org/MaterialsA

Gas sensors based on a noble metal-semiconductor are widely used and show a positive temperature response to hydrogen below 400 ℃. In our work, a catalytically activated hydrogen sensor is realized based on Pd decorated WO_3 nanoplates constructed by a solvothermal method. Insight into the role of Pd catalyst in outstanding performance is provided by comparing the sensing properties of this sensor with a traditional one made from the same pristine WO_3. The pure WO_3 sensor exhibited poor selectivity and low sensitivity to hydrogen. In contrast, the observed response of this sensor is up to 843 at a low operating temperature of 80 ℃, which is even greater than the WO_3 sensors at high temperature (250 - 400℃). In addition, the Pd-loaded WO_3 sensors show excellent selectivity in comparison to other common gases (CH_4, C_3H_6O, C_2H_6, C_3H_8O and NH_3). The significantly improved performance are well explained in terms of the adsorption-desorption mechanism and chemical kinetics theories. Furthermore, a interfacial model demonstrated in this report indicates that the interfacial barrier between WO_3 nanoparticles can be a novel effect for excellent gas sensing performance.

1. Introduction

Recently, hydrogen (H_2) -- a light, colorless, odorless and tasteless gas has acheived significant attention worldwide as a next-generation clean energy source. As a fuel, H_2 burns cleanly producing only environmentally-friendly water and no harmful by-products [1,2]. However, hydrogen has many potential risks such as a wide explosion concentration range (4-75%), low ignition energy (0.02mJ), large diffusion coefficient (0.61 cm^2s^{-1}), and large flame propagation velocity [3,4]. Therefore, detection and leakage control are challenge. As a result, the number of publications on hydrogen sensors has increased rapidly [5-9]. Simple binary metal oxides are generally used as materials for high sensitivity, fast-response H_2 sensors. Among these attempts, tungsten oxide (WO_3), with the high hydrophilic properties and low cost, have been widely investigated for applications in the fields of gas sensors, water splitting, batteries, photovoltaics, etc [10-13].

Numerous reports explain the growth of WO_3 nanostructures, including nanoparticles, films, nanowires [14,15], nanorods [16,17] and nanobelts [18]. In fact, morphology (WO_3 thin-film) is a very important parameter for obtaining stable and sensitive sensors. WO_3 is prepared using various techniques such as pyrolysis [19], sol-gel [20 - 22], sputtering [23 , 24], hydrothermal [25 , 26] and electrochemical anodizing methods [27]. However, like the majority of metal oxide-based gas sensors, pure WO_3 suffers from low sensitivity, poor selectivity and high working temperature (Table 1). In order to solve the above problem, Taguchi announced in 1963 the development of activated oxide such as oxides doped with platinoid catalyst,especially Pt and Pd [28-30], to lower the activation energy and accelerate the chemical reactions for rapid, high response [31-34]. By comparison, our work emphasizes the hydrothermal synthesis of Pd-loaded WO_3 nanoplates, which is a potentially superior technique with lower cost and lower temperature production for H_2 detection. Our work aims to describe the behavior of a gas sensor obtained by a Pd-loaded WO_3 nanostructure pasted onto ceramic tube. Results show that the catalytic activity of the Pd nanoparticles (NPs) is crucial. Enhancing the interaction between H_2 molecules and the sensing surface and decreasing the operating temperature to 80□ are the key points for improving H_2 gas-sensing performance. This paper investigates the operating temperature of the sensor and illustrates the negative temperature coefficients through an adsorption-desorption theoretical model. This effort will undoubtedly enable further research in the development of practical high-sensitivity gas sensors.

Table 1. Sensor response (Pd-WO_3) for the optimization conditions

sensing materials	H_2 conc.(vol%)	R_{gas}/R_{air}	Working temperature (°C)	Reference

2.5-nm Pd/11.2-nm WO_3 /IDEs/SiO_2/Si	2%	$4.77*10^4$	80	35
Pd-WO_3 nanolamellae	200ppm	69	180	36
Pd-WO_3 nanospheres	200ppm	41	180	40
Pd-WO_3 nanowires	200ppm	24.5	180	40
Pd-WO_3 nanostructure films	0.2%	407	350	37
Pd-WO_3 thin layers	500ppm	0.09	200	38

2. Experimental Details

2.1 Synthesis of WO_3 nanoplates.

WO_3 nanoplates were synthesized by a hydrothermal method reported elsewhere [39]. In a typical experiment, 0.15 g of citric acid and 0.25 g of ammonium tungstate hydrate ($(NH_4)_{10}H_2(W_2O_7)_6{\cdot}xH_2O$) were added into a 25 mL Teflon-lined autoclave followed by adding 15 mL of distilled water. Subsequently, the formed clear solution was kept under an intense ultrasonic treatment with a rated power of 100 W to form a uniform solution. Meanwhile, 100 uL of hydrochloric acid (37%) was added drop by drop. Ten minutes later, the resulting solution was transferred to Teflon-lined stainless autoclave and kept at 120◦C for 24 h. After cooling down to RT, the resulting solid products were collected by centrifuging at 8000 rpm and washed five times with distilled water and ethanol and dried in an electronic oven at 70◦C for 10 h. Finally, the as-prepared hydrate was annealed at 600◦C for 2h in air with a heating rate of 2◦C /min to obtain the WO_3 nanoplates.

2.2 Synthesis of Pd-WO_3 nanoplates.

The Pd decoration were conducted under thermodynamic control, using iodide ions as a strong adsorbate and polyvinyl pyrrolidone (PVP) as the capping agent [40,41]. In a typical synthesis, 12 mg of $PdCl_2$, 160 mg of PVP (K30), 360 mg of $NaI{\cdot}2H_2O$ and 2 mL of distilled water were added in sequence to a beaker containing 10 mL of N,N-dimethyl formamide (DMF). The resulting homogeneous solution was obtained after 10 min of stirring and then transferred into a Teflon-lined autoclave. Afterwards, 80 mg WO_3 was added to the liner followed by an intense ultrasonic treatment for 30 min. Then the liner was sealed and kept at 150□ for 480 min. After cooling down to RT, the resulting solid products were collected by centrifuging and washed with DMF and ethanol for further use.

2.3 Fabrication and measurement of hydrogen sensor

The sensors were fabricated using thin-films prepared from a powder suspension of as-synthesized Pd/WO_3 NPs. First, the nanoplates were ultrasonically dispersed in ethanol for 30 min and dried at 70°C for 1 h. Then, the material were dispersed in terpilenol, formed into a slurry, and slightly grinded before fabricating the sensors with two Au electrodes placed on the tube and a heating resistance coil inserted in the tube. No conductive binder was added. The schematic diagram of a typical gas sensor is shown in Figure 1. The sensing measurements were performed on a ZhongKe NS-4003 smart sensor analyzer (Beijing ZhongKe Micro-Nano Networking Technology Co., Ltd.) by monitoring the variation of the DC conductance. Testing was performed across a wide range of industrially relevant conditions: H_2 concentrations ranged from 0.1 to 0.5 vol% (balanced in synthetic air) while the operation temperatures ranged from 25 to 400°C. The ambient relative humidity is 50%.

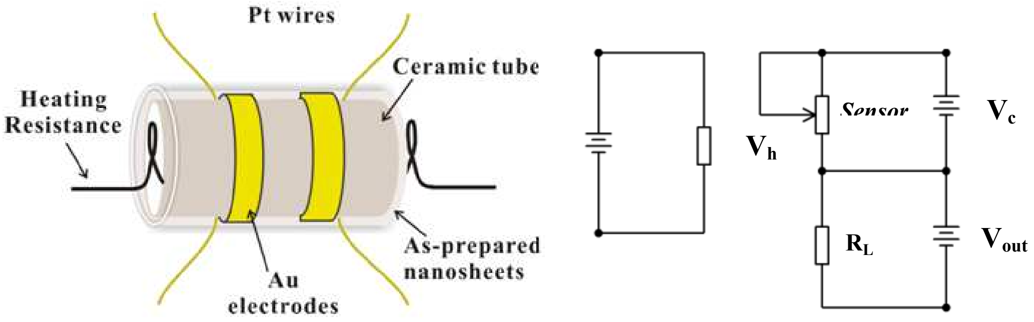

Fig. 1 Schematic diagram showing the structure of a typical Pd/WO_3 NPs gas sensor and test principle of the gas sensing measurement system (V_h: heating voltage; V_c : circuit voltage; V_{out}: signal voltage and R_L: load resistor).

2.4 Characterization

All chemicals used in this work were purchased from Sinoplarm Chemical Reagent CO.LTD and used without further purification. Deionized water was used throughout the experiment. Scanning electron microscopy (SEM) images were recorded on Hitachi S4800 scanning electron microscope. A FEI Tecnai F30 microscope operating at 300 kV was used for transmission electron microscopy (TEM) and high-resolution transmission electron microscopy (HRTEM) characterizations. X-ray powder diffraction (XRD) data of the as synthesized materials were collected on a Philips X'pert pro diffractometer using Cu-Kα radiation at 40kV and 30mA.

3. Results and discussions

3.1 Characterization of sensor material

Fig.2 contains typical SEM images displaying the general morphologies of as-grown WO_3 nanoplates. The product is composed of a large number of square-like nanoplates with good mono-dispersity. Fig.2a gives a low-magnification view of the WO_3. It is notable that all the nanoplates are roughly uniform, and the average diameter of the cubes is approximately 150 nm and a platelet thickness of 30 nm. Furthermore, a high-magnification image, as shown in Fig. 2b, also confirms the square-like nanostructures of the product. Some irregular sizes and shapes are also present. As previous research shows, WO_3 can exist in different forms and its crystal phase changes are reversible with temperature[42]. In this experiment, synthesized WO_3 presents a monoclinic phase as shown by X-ray diffraction (XRD) analysis.

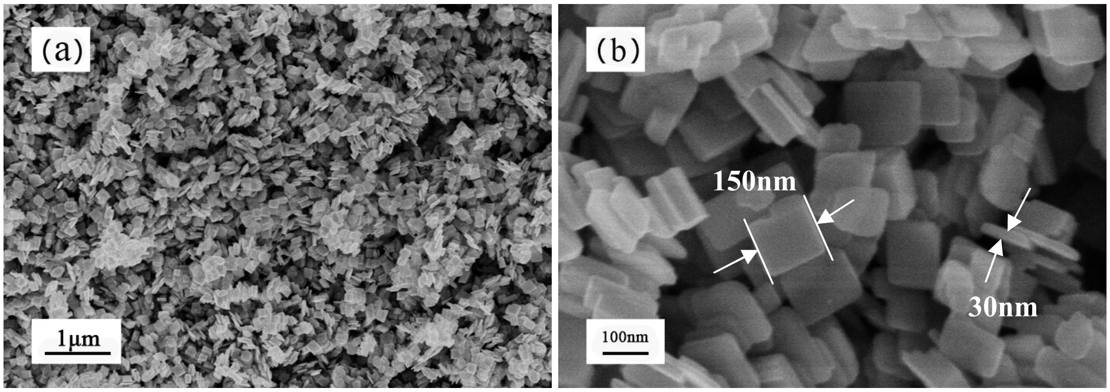

Fig. 2 SEM images showing the spherical morphology of WO_3. (a) Low-magnification images. (b) High-magnification images.

XRD was used to investigate the phase structures and purity of the as-prepared product. Fig.3 shows the typical patterns of pure WO_3 nanoplates. All the sharp diffraction peaks indicate the high crystalline quality of WO_3 nanoplates. Similarly, the reflection peaks in the figure indicate the monoclinic WO_3 with lattice constants of a =7.3060 Å; b =7.5400 Å; c =7.6920 Å; α= 90.0000°; β= 90.8810° (JCPDS card no.72-0677). No other clear, sharp peaks coincide with the peaks of other impurities, suggesting that the as-prepared nanoplates are of high phase purity of .

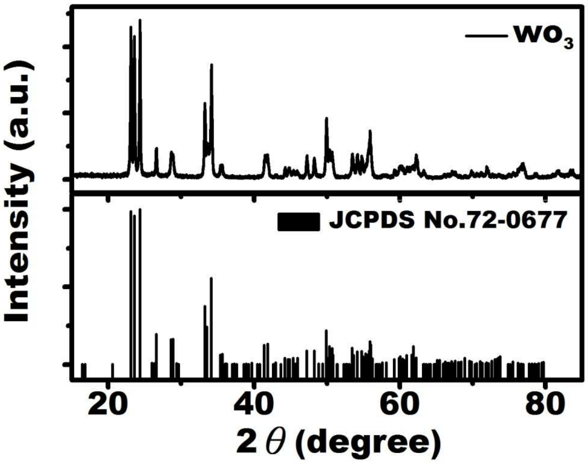

Fig. 3 XRD patterns of WO_3 nanoplates (references from ICDD database).

The SEM morphology in Fig. 4a indicates most Pd NPs are directly attached to the surface of the WO_3 nanoplates. This phenomenon is believed to play an important role in defining the performance of the reported sensors. The formation of Pd grown on the substrate of WO_3 nanoplates has platelike structures that are similar to the pure structures shown in Fig. 2a. TEM images (Fig.4c, 4d) further confirm the reliability of the decorating procedures. Fig. 4d shows a typical HRTEM image in which the lattice structures of the nanoparticles have an average diameter of approximately 15 nm. The spacing between two adjacent lattice planes is 0.224 nm, corresponding to (111) planes of Pd. The clear black peaks in the elemental energy spectra (Fig.4e) confirm that tungsten, oxygen and palladium, are the only detected elements.

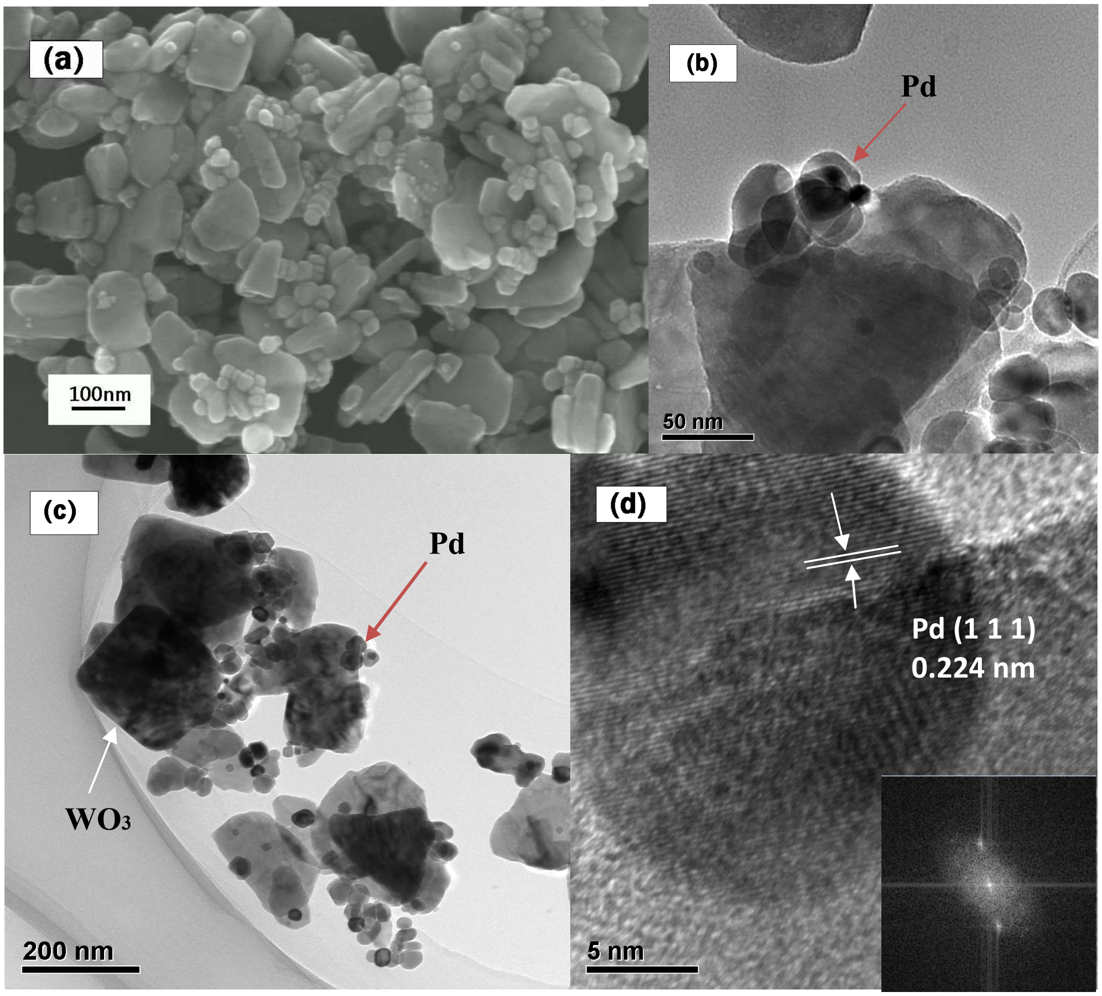

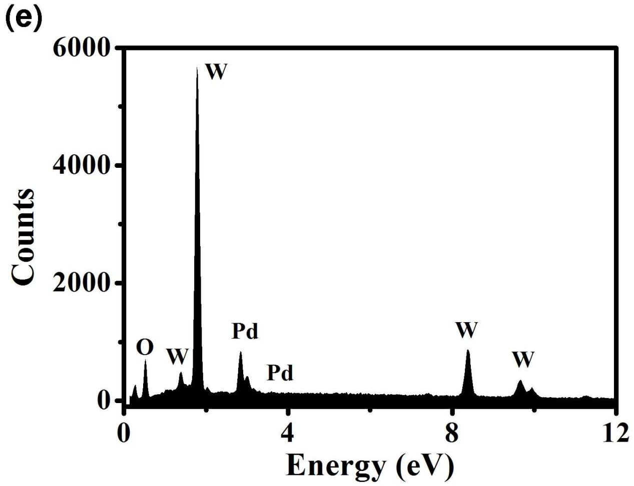

Fig.4 (a) SEM image and (b,c) TEM images of the Pd-loaded WO_3 nanoplates; (d) HRTEM lattice images of Pd -loaded WO_3 nanoplates, the inset is the fast Fourier transform (FFT) of the image; (e) EDS spectrum of the Pd decorated WO_3 nanoplates.

3.2 Response to hydrogen.

Hydrogen sensing performance is measured in ambient air at working temperature ranging from 25 to 400 °C at 50% relative humidity. The concentrations of hydrogen are varied from 0.1 to 0.5 vol%. Transient response curves of the sensor (composed of pure WO_3 and Pd-decorated WO_3) at the optimal temperature of 80°C are shown in Fig.5. The rectangle-shaped response and recovery curves indicate the sensor's excellent hydrogen response and rapid reaction rate. Exposing the sensor to H_2 significantly increases conductance and then reaches saturation. After removal of H_2, the conductance approaches its initial value. In contrast, the sensor fabricated from pure WO_3 nanoplates has little response to H_2 even when the concentration is increased to 0.5 vol%.

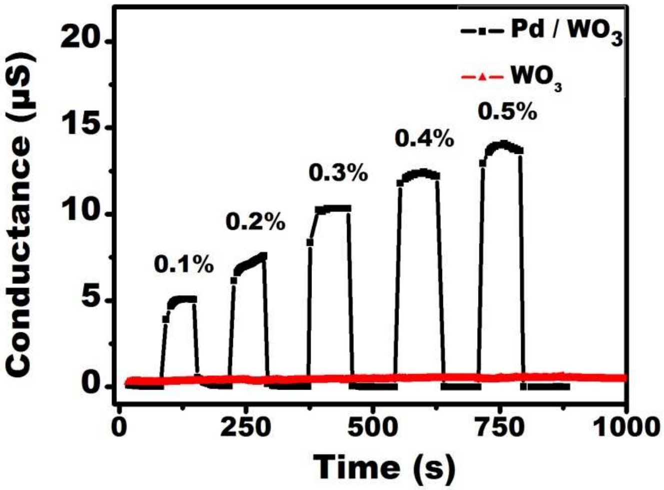

Fig. 5 Transient response curves of the sensor made from WO_3 and Pd/WO_3 with different H_2 concentrations at 80℃.

Fig. 6a shows the response-recovery time of the modified WO_3 sensor due to H_2 concentrations ranging from 0.1 to 0.5 vol%. The response time is defined as the period in which the sensor output variation reaches its steady state equilibrium value during exposure to gas. Recovery time is the period after gas removal in which the output reaches 100% of the final value. At 0.1 vol% concentration, the response and recovery times are 42.8 and 48.5 s, respectively. The results reveal that with the increase of H_2 concentration, the response and recovery times both show a sharp decrease. This phenomenon may be due to the presence and penetration of sufficient gas molecules on the surface of the Pd-loaded WO_3, which causes more reactions to occur 43. Therefore, the sensor requires a shorter response and recovery times to reach equilibrium.

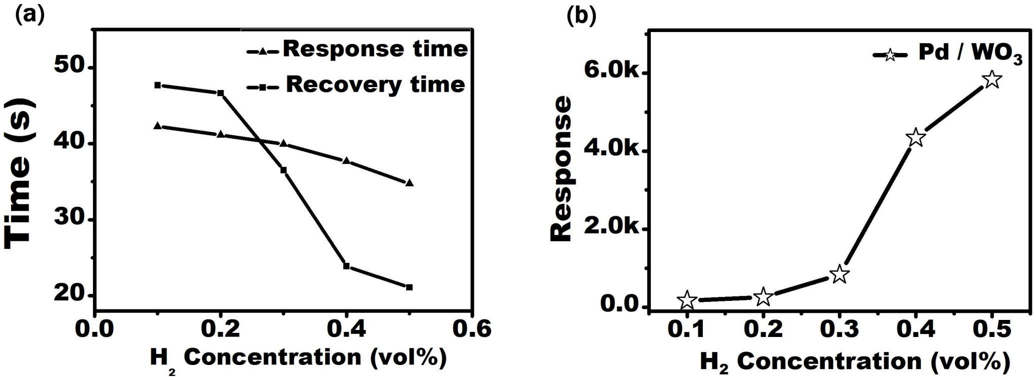

Fig. 6 Curves of (a) response and recovery time and (b) response of Pd-WO3 sensor vs. H2 concentration at 80℃.

The sensor response is defined as Response = R_{air} / R_{gas} , where R_{air} is the resistance in air and R_{gas} is the measured resistance in the presence of the test gas. Fig. 6b shows the relationship between the response of the sensor and the H_2 concentration from 0.1 to 0.5 vol%. Increasing the concentration accelerates the response, even at a low concentration of 0.1 vol%, the sensor has a high sensitivity of 169.3.

3.3 Selectivity

Variations in the electrical conductance due to gas adsorption are measured on both pure and Pd-activated WO_3 nanoplates. Methane (CH_4), acetone (C_3H_6O), ethane (C_2H_6), isopropyl alcohol (C_3H_8O), ethane (C_2H_6) and ammonia (NH_3) are five common gases (0.05vol%) used as probe molecules to investigate the cross-sensitivity of the sensor at an operating temperature of 80°C (Fig. 7a) and 400°C (Fig. 7b). Compare with the conductance change to 0.05vol% H_2 at 80°C, the Pd decorated WO_3 sensor's response to other gases are negligible. The pure WO_3 sensor shows low response to H_2 and the others. When the temperature increased to 400°C, the oxygen ions on the pure WO_3 NPs seem to highly active since whether hydrogen or any of hydrocarbon gases can induce an obvious response, whereas, Pd-loaded WO_3 nanoplates do not show any notable response to other gases, confirming the high H_2 selectivity.

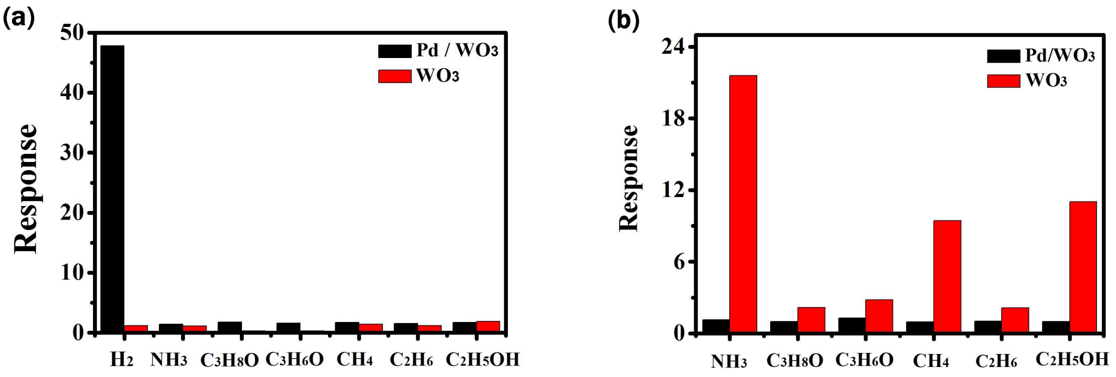

Fig. 7 Response curves to 0.05vol% different gases at (a) 80°C and (b) 400°C.

An appropriate amount of a noble metal has been shown higher catalytic activity and the consumption of a larger amount of oxygen adsorbates at lower temperature. As an electron donors, hydrogen molecules need to be dissociated into more active hydrogen atoms, then the reaction of them with oxygen ions can take place. Since the work function of Pd (5.6eV) are much larger than the electron affinity of WO_3 (3.3eV), net electron transfer from the semiconductor to metal will take place if the Pd NPs and WO_3 NPs come into contact, forming the nano-Schottky junction at the MS interface and acting as an "electron bath", which greatly enhance the catalytic performance for Pd nanocrystals[44].

3.4 Temperature effect

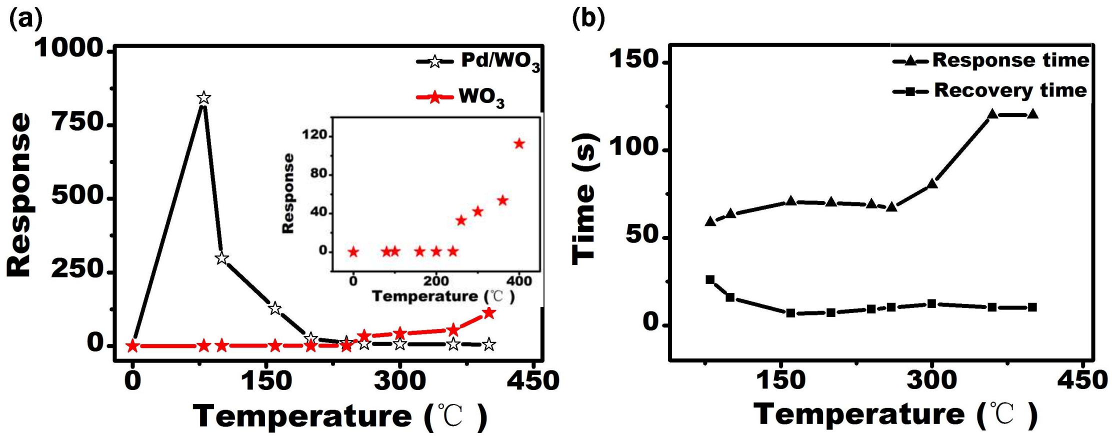

Fig. 8 (a) The corresponding response of Pd-loaded WO_3 and pure WO_3 toward H_2 gas at 0.3 vol% at different operating temperature, the inset is the amplified pure WO_3 response ; (b) Response and recovery time of Pd-loaded WO_3 thin film upon operating temperatures from 80 to 400 ◦C.

Fig. 8a shows that Pd-loaded WO_3 gas sensors achieve a maximum sensitivity of 843 at 80°C, while the pure WO_3 sensor responds only negligibly. With increasing operating temperature, the response of the Pd-loaded WO_3 sensor significantly decreases. Moreover, in comparison with the pure WO_3 sensor, the Pd-decorated WO_3 sensor is approximately eight hundred times more sensitive at the optimal temperature (80°C). Thus, the addition of Pd NPs not only enhanced sensing ability, but also significantly reduced the operating temperature. Additionally, the pure WO_3 sensor reveals a sharp response as the temperature increases to 250°C (inset of Fig.8(a)). Due to the heating process, the oxygen ions on the WO_3 surface are highly active; this increases the activation energy, producing a clear improvement. Subsequently, as reveals in Fig. 8b, there is a notable increase in response time of the Pd-loaded WO_3 sensor when the operating temperature is increased. When the temperature was increased to 250 °C, the sensor showed a longer response time and shorter recovery time.

The negative temperature coefficient effect of the Pd-loaded WO_3 sensor has many implications. As a recent theoretical study shows, oxygen ion species ionosorbed on the surface of an oxide depend on the operation's temperature[45]. In the case of pure WO_3 nanoplates, it is assumed that the surface oxygen vacancies play the role of chemisorption sites in the presence of oxygen. Oxygen molecules are adsorbed on the WO_3 surface through two mechanisms: physisorption and chemisorption. At low temperature, the oxygen molecules are physisorbed on the oxide surface, and the bond is weak, leading to a comparatively small response to hydrogen (see in Fig.5). As the temperature rises, the bond between chemisorbed oxygen ions and the WO_3 surface strengthens. The oxygen species dissociate into more active molecules and atomic ions [46]

$$O_{2\,gas} \leftrightarrow O_{2\,ads} + e^- \leftrightarrow O_2{}^-{}_{ads} + e^- \xleftrightarrow{KT} O^-{}_{ads} + e^- \xleftrightarrow{KT} O^{2-} \qquad (1)$$

where O_2 gas is a gaseous oxygen molecule in an ambient atmosphere. The ionization of oxygen molecules occurs due to the capture of electrons from the conduction band of WO_3.

These oxygen molecules act as electron acceptors, resulting in a deep electron depletion region with reduced electron mobility near the oxide's surface. This phenomenon enhances the surface potential and work function.

Surface-controlled, oxide-semiconductor gas sensors demonstrate a specific property. It is asserted that gas adsorption on a material's surface modifies the density of free electrons close to the surface, causing variations in resistance. WO_3 is a wide-band gap semiconductor. As a result, its n-type conductivity is due to the presence of bulk oxygen vacancies. Two varying densities of the vacancies associated with two distinct donor levels are needed to explain the two types of W-O bonds of the WO_3 crystalline structure [47]. When the WO_3 sensor is exposed to hydrogen, the surface oxygen ions react with the dissociated H atoms and create a number of carriers. This leads to a decrease in the potential barrier height and, hence, a drop in resistance[48]. The hydrogen dissociative adsorption depends on the height of the activation energy barrier for breaking the H-H bonds. According to the Polanyi rules, the molecule needs to encounter a considerable activation energy barrier. As the operating temperature of the pure WO_3 sensor increases, the activation energy increases and accelerates the reaction (2), resulting in a significant increase in conductivity (Fig.8a).

$$2H + O_2^- \leftrightarrow H_2O + e^- \qquad (2)$$

The sensing mechanism of the Pd-loaded WO_3 nanoplates is modeled by two different mechanisms : the Adsorption-desorption gas mechanism and chemical kinetics theory.

First, as shown in Fig.5, when H_2 gas flows in, the hydrogen molecules are dissociated into additional H atoms on the surface by the Pd catalyst. Next, the hydrogen atoms spill-over and diffuse along the surface of the WO_3 nanoparticles. The chemisorption of hydrogen on the surface is exothermic and provides a small activation energy for subsequent surface diffusion[49]. The H atoms form equivalent bonds with lattice oxygen ions of WO_3 on the surface. The adsorption process is as follows：

$$H_{2\,gas} \xrightarrow{Pd} 2H_{ads} \qquad (3)$$

$$2H_{ads} + O_2^{-} \leftrightarrow H_2O + e^{-} \qquad (4)$$

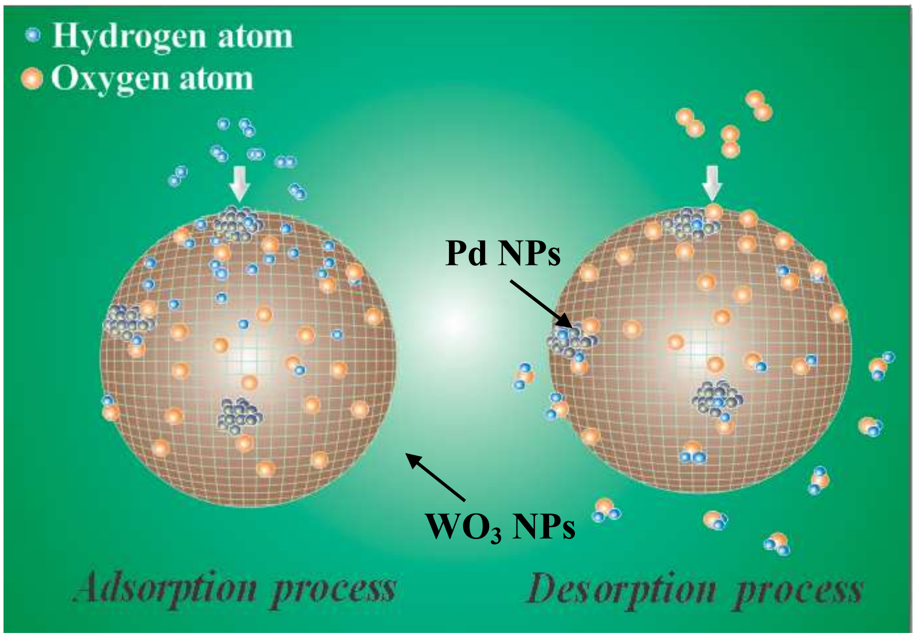

Fig.9 Schematic diagram of the adsorption-desorption mechanism of the Pd decorated WO_3 sensor

As the inflow of hydrogen ceases, the density of the surface oxygen increases, and the resultant H_2O molecules are removed in the form of H_2O vapor. The electrons return to the WO_3 molecules, varying the resistance of the sensor. This results in a decrease of the energy barrier at the grain. Furthermore, for the reason that Pd is a superior oxygen-dissociation catalyst (compared to WO_3), the oxygen molecules in the air are adsorbed chemically by Pd nanoparticles and diffuse to the WO_3 surface in a "spillover effect" (catalysis literature term). The oxygen atoms, occupying the vacancies, are then able to capture electrons, forming new bonds with W ions.

The adsorption of dissociated H atoms on the oxide surface differs from that reported in the previous In_2O_3 sensor research [34]. In this paper, the reaction of hydrogen with oxygen (from the lattice) leads to a partial reduction of WO_3 and forms hydrogen tungsten bronzes

(H_xWO_3, x~ 0-1). Catalytic H atoms are reduced as the surface electron density of WO_3 decreases [50].

$$\chi H_{ads} + WO_3 \rightarrow H_\chi WO_3 \qquad (5)$$

A reversal reaction occurs when H_2 gas is purged from the system at elevated temperatures in the presence of air. An oxidizing agent is required to reform the WO_3 matrix, resulting in the dissociation of the water molecules[51].

$$H_\chi WO_3 + 0.25\chi O_2 \rightarrow WO_3 + 0.5\chi H_2O \qquad (6)$$

Both the adsorption and desorption reactions lead to an increase in conductivity (in contact with hydrogen) and lower the width of the depletion barrier. With the Pd catalyst, the number of carriers in the conducting band changes, which enhances the oxygen ions on the WO_3 surface and forms an electron depletion region. For the H_2/Pd-WO_3 reaction system, when gas molecules come into contact with a solid, the stability of the system tends toward a minimum energy state. As the temperature increases, there is an increase in the molecular kinetic energy, and a decrease in the potential energy reduces as a result. At high temperatures, the potential energy between the molecules decreases and the Pd-H bond rupture. Consequently, the gas desorption rate increases more rapidly (outpacing the adsorption rate). Therefore, the coverage of the chemisorbed species shows a maximum value with increasing temperature and reveals a negative coefficient for hydrogen[52].

An alternative theory to explain the response to H_2 of a Pd-decorated WO_3 sensor is the chemical reaction kinetics theory.

The ability of a reacting species to overcome a free energy barrier preventing a reaction is commonly modeled by the Arrhenius equation. For most chemical reactions, including primitive reaction and the primitive action, the Arrhenius equation gives the dependence of rates, K, of a chemical reaction on the absolute temperature T (in Kelvin):

$$K = A \cdot \exp^{-\frac{Ea}{RT}} \quad (7)$$

Taking the natural logarithms of the Arrhenius equation results in the following formula:

$$InK = InA - \frac{Ea}{RT} \quad (8)$$

This equation shows that the rate constant decreases exponentially as 1/T increases. The inflection point occurs at T = E_a/2R. In conclusion, the adsorption-desorption mechanism reveals that the sensor's response decreases with increasing temperature, while the chemical kinetics rate has a positive temperature coefficient. When the two opposing temperature effect mechanisms attain a balance, the system achieves an optimal response. Furthermore, lnK varies directly in proportion to the activation energy. The activation energy of the chemical reaction on the sensor's surface strongly affected the response. For the pure WO_3 sensor, a higher activation energy is required to react, therefore, the operating temperature of the reaction is high. In the presence of Pd, the WO_3 sensor provides a reaction path with a lower activation energy, achieving a maximum response at a low temperature.

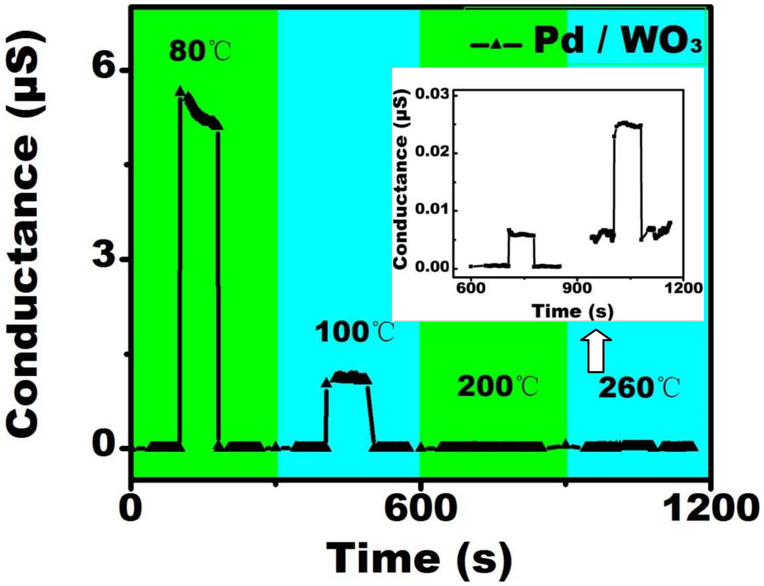

Fig. 10 Temperature-dependent response curves to 0.05 vol% H_2 (inset shows the response curves of the sensor at 200 and 260 ℃).

Fig. 10 shows plots of the typical response curves as a result of different temperature values varying from 80 to 260 °C. As Fig. 8 illustrates, the response time of the pure WO_3 sensor demonstrates an obvious increase when the temperature reaches 250°C. Correspondingly, this same phenomenon is exhibit in the Pd-loaded WO_3 sensor (inset of Fig.10). With increasing temperature, the thermal energy of the electrons overcomes the charge depletion layer in $WO_{3.}$ The surface oxygen ions appear highly active; therefore, hydrogen induces an obvious response. However, in contrast with Pd catalysis, this electron transfer and conductance change is very small.

3.5 Inter-facial barrier

The contacts between the WO_3 nanoparticles are examined. The samples are approximately 150 nm in length and up to 30 nm in thickness. As Fig.11 shows, this contact between the outer ends of the nanoplates leads to the formation of junctions [53]. The surface energy barrier is given by the equation: $G = G_0 \exp(-\phi_s / k_b T)$, where G_0 is the conductance of the grain in air [54]. Oxygen species react with the dissociated H atoms on the surface of the WO_3 nanoplates. This action causes the release of trapped electrons that then return to the oxide, lowering the depletion region from W_1 to W_2 (see Fig.11). The interfacial barrier decreases by $\Delta\phi_s = \phi_0 - \phi_s$. The conductance can be approximately expressed by $G_s = G_0 \exp\{-\Delta\phi_s / k_b T\}$, and accordingly, $G_s = SG_0 \exp\{-\phi_0 / k_b T\}$, therefore, $\phi_s = \ln s \cdot k_b T$ .When exposed to 0.3 vol% hydrogen at 80°C, the potential barrier decreases by ~0.21eV. At low temperature, such a large contact-controlled sensing modulation guarantees the high sensitivity demonstrated.

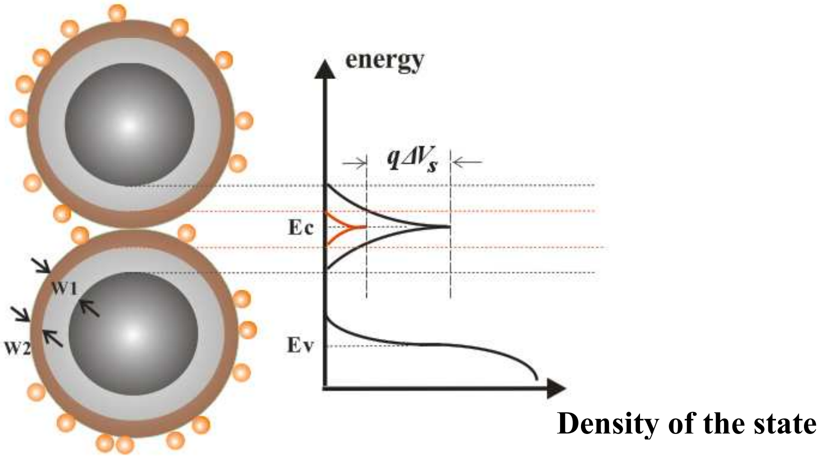

Fig. 11 Energy barrier caused by the hydrogen an the interface of the sensor

4. Conclusion

In summary, a simple method for the synthesis of Pd-loaded WO_3 nanoplates sensors was developed and explored. The SEM and TEM data prove that Pd NPs are successfully loaded onto WO_3. The electronic property demonstrates that the presence of Pd on the WO_3 surface enhances the sensitivity of the sensor and lowers the optimum operating temperature at low concentrations. Taking advantage of contact-controlled sensing and the spillover effect, we achieved superior selectivity and high sensitivity. Furthermore, the sensor exhibits negative temperature behavior, which is modeled successfully with the adsorption-desorption mechanism and chemical kinetics theory. Therefore, the excellent performance of the Pd/WO_3 sensors at low temperature strongly suggests a promising method for the development of a novel semiconductor gas sensor.

Acknowledgments

This research was partly supported by the National Natural Science Foundation of China (Grant No. 61376073) and the Fundamental Research Funds for Xiamen University (Grant No. 201412G010).

Notes and references

[a] Department of Physics/Pen-Tung Sah Institute of Micro-Nano Science and Technology, Xiamen University, Xiamen, China.
E-mail: thwang@xmu.edu.cn; liqiuhong2004@hotmail.com.
Fax: +86-0592-2187196; Tel: +86-0592-2183063.

---

1 Muhammad Z. Ahmad, Vladimir B. Golovko, Rohul H. Adnan, Faridah Abu Bakar, Jan-Yves Ruzicka, David P. Anderson, Gunther G. Andersson. *International Journal of Hydrogen Energy*, 2013, 38, 12865.

2 Sunil K. Arya, Subramanian Krishnan, Hayde Silva, Sheild Jean and Shekhar Bhansali. *Nanoscale,* 2012, 137, 2743.

3 Al-Hardan NH, Abdullah MJ, Aziz AA. *International Journal of Hydrogen Energy,* 2010, 35, 4428.

4 Sumida S, Okazaki S, Asakura S, Nakagawa H, Murayama H, Hasegawa T. Sens. Actuators, B, 2005, 108, 508-514.

5 Shaposhnik D, Pavelko R, Llobet E, Gispert-Guirado F, Vilanova X. *Procedia Engineering,* 2011, 25, 1133.

6 Jimenez VM, Espinos JP, Gonzalez-Elipe AR. *Sens. Actuators, B,* 1999, 61, 23.

7 Yoo KS, Park SH, Kang JH. *Sens. Actuators, B,* 2005, 108, 159.

8 S. Okazaki, H. Nakagawa, S. Asakura, Y. Tomiuchi, N. Tsuji, H. Murayama, M. Washiya. *Sens. Actuators, B,* 2003, 93, 142.

9 Baik NS, Sakai G, Miura N, Yamazoe N. *Sens. Actuators, B,* 2000, 63, 74.

10 Granqvist CG. *Solar Energy Materials and Solar Cells,* 2000, 60, 201.

11 Deb SK. *Solar Energy Materials and Solar Cells,* 2008, 92, 245.

12 Huang K, Pan Q, Yang F, Ni S, Wei X. *Journal of Physics D-Applied Physics,* 2008, 41, 175305.

13 Zheng HD, Tachibana Y, Kalantar-zadeh K. *Langmuir,* 2010, 26, 19148.

14 Polleux J, Gurlo A, Barsan N, Weimar U, Antonietti M, Niederberger M. *Angewandte Chemie International Edition ,* 2005, 45, 261.

15 Baek Y, Yong K. *Journal of Physical Chemical C,* 2007, 111, 1213.

16 Carreon MA, Guliants VV. *European Journal of Inorganic Chemistry,* 2005, 1, 27-43.

---

17 Aswani Yella, Muhammad Nawaz Tahir,Stefan Meuer, Rudolf Zentel, Rüdiger Berger, Martin Panthöfer and Wolfgang Tremel. *Journal of the American Chemical Society,* 2009, 131, 17566.

18 Deliang Chen, Hejing Wen, Huimin Chen, Hailong Wang, Rui Zhang, Hongliang Xu, Daoyuan Yang, Hongxia Lu. *Materials Chemistry Physics,* 2009, 116, 507.

19 Samerjai T, Tamaekong N, Liewhiran C, Wisitsoraat A, Tuantranont A, Phanichphant S. *Sens. Actuators, B,* 2011, 157, 290.

20 Breedon M, Spizzirri P, Taylor M, Plessis J, McCulloch, Zhu J, Yu L, Hu Z, Rix C, Wlodarski W, Kalantar Zadeh K. *Crystal Growth and Design,* 2010, 10, 430.

21 Ippolito SJ, Kandasamy S, Kalantar-zadeh KK, Wlodarski W. *Sens. Actuators, B,* 2005, 108, 154.

22 C. Zhang, A. Boudiba, C. Navio, C. Bittencourt, M. G. Olivier, R. Snyders, M. Debliquy. *International Journal of Hydrogen Energy,* 2011, 36, 1107.

23 Shen Y, Yamazaki T, Liu Z, Meng D, Kikuta T, Nakatani N. *Thin Solid Films,* 2009, 517, 2069.

24 Penza M, Tagliente MA, Mirenghi L, Gerardi C, Martucci C, Cassano G. *Sens. Actuators, B,* 1998, 50, 9.

25 Boudiba A, Zhang C, Umek P, Bittencourt C, Snyders R, Oliver MG.*International Journal of Hydrogen Energy,* 2013, 38, 2565.

26 Ou JZ, Ahmad MZ, Latham K, Kalantar- zadeh K, Sberveglieri G, Wlodarski W. *Procedia Engineering,* 2011, 25, 247.

27 Calavia R, Mozalev A, Vazquez R, Gracia I, Cane´ C, Ionescu R, Llobat E. *Sens. Actuators, B,* 2010, 149, 352.

28 Yamauchi, Shigeru, ed. Chemical Sensor Technology. Vol. 4. *Elsevier*, 1992.

29 Liu B, Cai D, Liu Y, Li H, Weng C, Zeng G, LiQ, WangT. *Nanoscale*, 2013, 5, 2505.

30 Su Hui Lim, Boya Radha, Jie Yong Chan, Mohammad S. M. Saifullah, Giridhar U. Kulkarni and Ghim Wei Ho. *ACS Apply Material Interfaces,* 2013, 5, 7274.

31 A. Kolmakov, D.O. Klenov, Y. Lilach, S. Stemmer, M. Moskovits. *Nano Letters,* 2005, 5, 667.

32 C. Bigey, G. Maire. *Journal of Catalysis,* 2000, 196, 224.

33 A. Georg, W. Graf, R. Neumann, V. Wittwer. *Solar Energy Materials and Solar Cells,* 2000, 63, 165.

34 Wang Yanrong, Liu Bin, Cai Daoping, Li Han, Liu Yuan, Wang Dandan, Wang Lingling, Li Qiuhong, Wang Taihong. *Sens. Actuators, B,* 2014, 201, 351.

35 Zhao M, Huang J, Ong C W.*International Journal of Hydrogen Energy,* 2013, 38, 15559.

36 Abdelhamid Boudiba, Chao Zhang, Polona Umek, Carla Bittencourt, Rony Snyders, Marie-Georges Olivier, Marc Debliquy. *International Journal of Hydrogen Energy,* 2013, 38, 2565.

37 Ghadiri E, Iraji zad A, Razi F. *Synthesis and Reactivity in Inorganic, Metal-Organic, and Nano-Metal Chemistry,* 2007, 37, 453.

38 Penza M, Martucci C, Cassano G. *Sens. Actuators, B,* 1998, 50, 52.

39 X.T. Su, F. Xiao, Y.N. Li, J.K. Jian, Q.J. Sun, J.D. Wang. *Materials Letters,* 2010, 64, 1232.

40 Xiaoqing Huang, Huihui Zhang, Changyou Guo Dr., Zhiyou Zhou Dr. And Nanfeng Zheng. *Angewandte Chemistry,* 2009, 121, 4902.

41 Mei Chen, Binghui Wu, Jing Yang, Nanfeng Zheng. *Advanced Materials*, 2012, 24, 862.

42 Boudiba A, Roussel P, Zhang C, et al. *Sensors and Actuators B: Chemical,* 2013, 187: 84-93.

43 Nasirian S, Milani Moghaddam H. *International Journal of Hydrogen Energy,* 2014, 39, 630.

44 M. Cargnello, V. V. Doan-Nguyen, et al. *Science,* 2013, 341, 771-773.

45 U. Pulkkinen , T. T. Rantala , T. S. Rantala , V. Lantto. *Journal of Molecular Catalysis A: Chemical,* 2001, 166 , 15 .

46 Diogo P. Volanti , Anderson A. Felix , * Marcelo O. Orlandi , George Whitfi eld. *Advanced Functional Materials,* 2013, 23, 14.

47 M. Bendahan, J. Guérin, R. Boulmani, K. Aguir.*Sens. Actuators, B,* 2007, 124, 24.

48 Z.A. Ansari, T.G. Ko, J.H. *IEEE,* 2005,5, 817.

49 Conner, W. C.; Falconer, J. L.Chem. ReV. 1995, 95, 759

50 Han Li, Bin Liu, Daoping Cai, Yanrong Wang, Yuan Liu, Lin Mei, Lingling Wang, Dandan Wang, Qiuhong Li and Taihong Wang. *Journal of Materials Chemistry A,* 2014, 2, 685.

---

51 Thanittha Samerjai, Chaikarn Liewhiran, Anurat Wisitsoraat, Adisorn Tuantranont, Chanitpa Khanta, Sukon Phanichphant. *International Journal of Hydrogen energy,* 2014, 39, 6120.

52 M.J. Madou, S. Roy Morrisson. *Academic Press,* 1989, 67.

53 P. Feng, Q. Wan, and T. H. Wang, *Appl. Phys. Lett.* 87, 213111 (2005).

54 T. Weis, R. Lipperheide, U. Wille, and S. Brehme, *J. Appl. Phys.* 92, 1411(2002).